IODP
INTERNATIONAL OCEAN
DISCOVERY PROGRAM

Data report: IODP Expedition 366 pore water trace element (V, Mo, Rb, Cs, U, Ba, and Li) compositions[1]

Check for updates

Contents

C. Geoffrey Wheat,[2] Trevor Fournier,[2] Claudia Paul,[2] Catriona Menzies,[3]
Roy E. Price,[4] Jeffrey Ryan,[5] and Olivier Sissman[6]

Abstract

International Ocean Discovery Program (IODP) Expedition 366 focused, in part, on the study of geochemical cycling, matrix alteration and transport, and deep biosphere processes in the Mariana subduction zone. This research was accomplished by sampling the summit and flank regions of three active serpentinite mud volcanoes in the Mariana forearc: Yinazao (Blue Moon), Fantangisña (Celestial), and Asùt Tesoro (Big Blue) Seamounts. These mud volcanoes represent a transect with increasing distance from the trench. Because these mud volcanoes discharge fluids and materials from the subduction channel, they provide a means to characterize thermal, geochemical, and pressure conditions within the seismogenic zone. Previous coring on Ocean Drilling Program (ODP) Legs 125 and 195 at two other serpentinite mud volcanoes (Conical and South Chamorro Seamounts, respectively) and piston, gravity, and push cores from several other Mariana serpentinite mud volcanoes add to this transect of deep-sourced material that is discharged at the seafloor.

Pore waters were squeezed from cored serpentinite materials to determine the composition of deep-sourced fluid from the subduction channel and to assess the character, extent, and effect of diagenetic reactions and mixing with seawater on the flanks of three serpentinite seamounts (Yinazao, Fantangisña, and Asùt Tesoro). In addition, two water-sampling temperature probe (WSTP) fluid samples were collected in two of the cased boreholes, each with at least 30 m of screened casing that allowed formation fluids to discharge into the borehole. Here we report shore-based Li, Rb, Cs, Ba, V, Mo, and U measurements of pore waters and one of the WSTP samples. The alkali metals were analyzed to constrain the temperature of reaction in the subduction channel. The other elements were analyzed to assess potential biogenic and diagenetic reactions as the serpentinite material weathers and exchanges with bottom seawater via diffusion. Results were generally consistent with earlier coring and drilling operations, resulting in systematic changes in the composition of the deep-sourced fluid with distance from the trench.

Introduction

One goal of International Ocean Discovery Program (IODP) Expedition 366 was to elucidate geochemical cycling within the subduction channel of the Mariana forearc system (see the **Expedition 366 summary** chapter [Fryer et al., 2018b]). Expedition 366 successfully cored the flank and summit regions of three Mariana forearc serpentinite mud volcanoes that are located along a transect with increasing distance from the trench and by inference with depth to the subducted Pacific plate (Figure **F1**). Previous scientific drilling during Ocean Drilling Program (ODP) Legs 125 and 195 at two other Mariana serpentinite mud volcanoes, Conical and South Chamorro Seamounts, respectively, as well as piston, gravity, and push cores from several other Mariana serpentinite mud volcanoes add additional geochemical data to this transect of active serpentinite mud volcanoes in the Mariana forearc (Fryer, Pearce, Stokking, et al., 1990; Salisbury, Shinohara, Richter, et al., 2002; Mottl et al., 2004; Hulme et al., 2010).

One of the expedition's primary objectives was to determine the composition of deep-sourced fluid to characterize thermal, geochemical, and pressure conditions within the subduction channel by sampling the summit region where newly deposited material is currently being delivered. A second primary objective was to assess the character, extent, and effect of diagenetic reactions and mixing with seawater on the flanks of three serpentinite mud volcanoes, thus

Figure F1. Locations of IODP Expedition 366 Sites U1491–U1498 and Site 1200 on South Chamorro Seamount superimposed on a regional bathymetric map. (From the Expedition 366 summary chapter [Fryer et al., 2018b].)
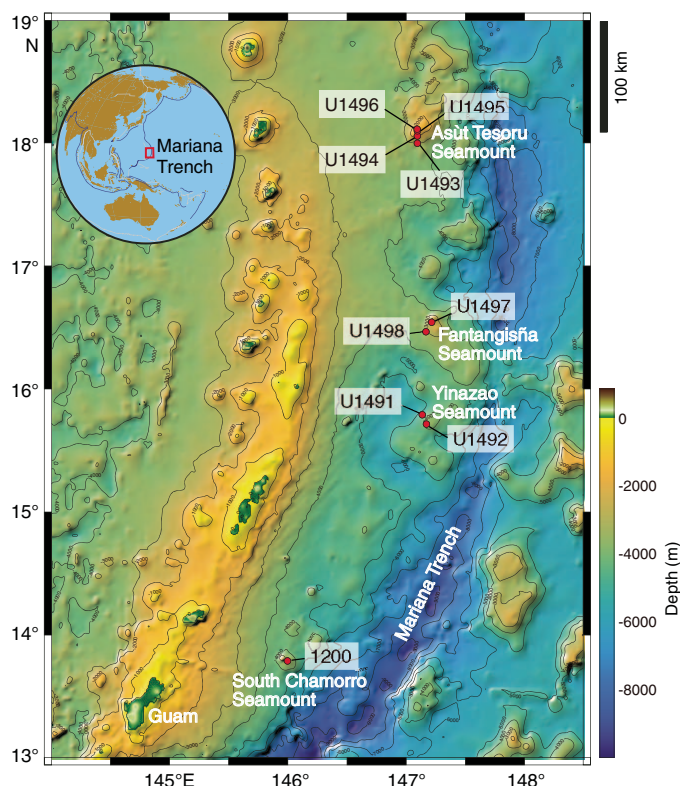
providing constraints for the extent of continued serpentinite reactions and potential microbial metabolic activity. To meet these two objectives, 149 whole-round samples were collected for pore water extraction. Extracted pore waters were analyzed shipboard, aliquoted into a range of containers, and preserved for shore-based analyses (see the **Expedition 366 summary** chapter [Fryer et al., 2018b]). In addition, two fluid samples were collected using the water-sampling temperature probe (WSTP) within two cased boreholes, each with screened casing that allows formation fluids to flow into the borehole while retaining the mud matrix (e.g., ODP Hole 1200C; Wheat et al., 2008).

Although pore waters were analyzed for many dissolved ions and gases at sea, shipboard instrumentation limits some critical analyses. This paper remedies this limitation by presenting results from analyses of trace elements, particularly Rb and Cs. These two elements constrained the temperature of the deep-sourced fluid, given their similar chemistries but different mobilization characteristics (e.g., Hulme et al., 2010). Lithium concentration data, another alkali metal, also is presented because many samples have concentrations that were below the detection limit afforded by the shipboard instrument. Other trace elements (V, Mo, Ba, and U) were measured and are presented to provide a gauge for potential reactions and diagenetic pathways on the flanks of the seamount.

Methods

Coring with the half-length advanced piston corer (HLAPC) was the primary method used to acquire material during Expedition 366 (see the **Expedition 366 methods** chapter [Fryer et al., 2018a]).

We also recovered material with extended core barrel (XCB) and rotary core barrel (RCB) coring. Recovered materials included serpentinite mudflows with clasts from the flanks of each of three edifices and pelagic sediment: Sites U1491 (Yinazao [Blue Moon] Seamount), U1493, U1494, U1495 (Asùt Tesoro [Big Blue] Seamount), and U1498 (Fantangisña [Celestial] Seamount) (Figure **F1**). The serpentinite mudflow matrix differed in color with depth and, although distinctly disturbed by flow-in during HLAPC and XCB coring, discrete horizons of clast content and matrix constituents remained in place. Serpentinite material also was recovered from the summit regions of each of the three cored mud volcanoes: Sites U1492 (Yinazao Seamount), U1496 (Asùt Tesoro Seamount), and U1497 (Fantangisña Seamount).

Serpentinite material and sediment for pore water analysis were immediately taken from the catwalk and placed in a refrigerator to cool samples to near (2°–5°C) the in situ temperature (see the **Expedition 366 methods** chapter [Fryer et al., 2018a]). Serpentinite and sediment samples were then extracted from the core liner in a nitrogen-filled glove bag, scraped to remove the outer contaminated rind, and placed into a titanium squeezer. The squeezer was removed from the glove bag and inserted into the press. Pore waters were expelled, filtered, aliquoted, preserved, and stored for a range of shore-based analyses. A total of 149 pore water samples and 2 WSTP samples were collected during Expedition 366. Unfortunately, not all of the whole-round samples provided sufficient fluids for shore-based analyses for each solute or isotope. Only the WSTP sample from Hole U1496C is included in this data set.

Analyses presented herein were conducted using the identical inductively coupled plasma–mass spectrometry (ICP-MS) and inductively coupled plasma–optical emission spectrometry (ICP-OES) methods that Mottl et al. (2004) and Hulme et al. (2010) used, thus ensuring continuity among data sets. Trace elements (V, Mo, Rb, Cs, U, and Ba) were analyzed on 103 samples using an ICP-MS with a 1:50 dilution in 3% ultra-pure nitric acid and standard machine settings (Table **T1**). Standards were matrix matched with bottom seawater from the eastern flank of the Juan de Fuca Ridge (Wheat et al., 2010). This seawater and a blank were analyzed about every 8 to 10 samples to account for machine drift. The average concentration of this bottom seawater and the standard deviation are listed in Table **T1**.

The lack of sensitivity in the Li measurements at sea led us to analyze 127 samples on an ICP-OES with a 1:25 dilution in 3% ultra-pure nitric acid utilizing standard axial machine settings (Table **T1**). Concurrent with this measurement, we also measured B, Ba, Mn, Fe, Si, and Sr, and we measured Ca, Mg, K, Na, and S on a separate aliquot with a 1:100 dilution. These analyses were conducted to confirm that shipboard results were consistent with results that were generated during prior work (e.g., Mottl et al., 2004; Hulme et al., 2010). As expected, results from these shore-based analyses and shipboard results agree within analytical precision. Duplicate shore-based results are not presented because the entire data set was not analyzed and the IODP database already includes measured values.

Deep-sourced fluid compositions for the three seamounts that were drilled during Expedition 366 were calculated based on pore water data from the summit boreholes for which the fluid composition reaches an asymptotic composition with depth. Such profiles are consistent with deep-sourced fluids that upwell faster than the surrounding serpentinite matrix (e.g., Fryer, Pearce, Stokking, et al., 1999; Mottl et al., 2003, 2004; Hulme et al., 2010). Concentrations calculated for the deep-sourced fluid for Yinazao Seamount were generally based on the average concentration of pore waters from

Table T1. Pore water chemical data arranged by distance from the trench. **Download table in CSV format.**

Table T2. Summary of deep-sourced fluids. * = Expedition 366 data are the average of deeper samples at the summit sites, as described in the text. Other data are from Hulme et al., 2010. **Download table in CSV format.**

Serpentinite seamount	Distance to trench (km)	pH	Alkalinity (mmol/kg)	Mg (mmol/kg)	Ca (mmol/kg)	Sr (µmol/kg)	Sulfate (mmol/kg)	Ba (µmol/kg)	B (µmol/kg)	Li (µmol/kg)	Na (mmol/kg)
Bottom seawater	0	8.1	2.3	52.4	10.2	90	28	0.140	410	26	466
Yinazao (Blue Moon)*	55	10.7	1.4	0.9	58	750	23.9	0.22	0.2	4.7	361
Cerulean Springs	60	10.8	2.3	0	49.5	320	8.5	0.297	15	2.1	220
East Quaker	61	10.7	3.1	0.2	74.8		6.9				360
Fantangisña (Celestial)*	62	~10.8	<0.5	<2	>82	>630	<8	~0.8	<1	~12	~400
NE Quaker	63	>8.3	<1.3	20	>33		<23				<420
Pacman	70	>8.9	<1.0	44	<6.9	<56	<25	<0.118	<387	>30.3	464
Quaker	76	9.2	0.8	0.5	18.1	205	23	0.125	830	119	461
Baby Blue	72	>9.0	<1.0	40	<6.9	<61	<22	0.216		>31	>489
Asùt Tesoro (Big Blue)*	72	12.5	73	0.8	0.1	13	30	0.07	1,070	4	640
South Chamorro	78	12.5	62	0	0.3	10	28	0.40	3,000	0.4	610
Conical	86	12.5	52	0.1	1	20	46	0.10	3,900	1.6	390

Serpentinite seamount	Distance to trench (km)	K (mmol/kg)	Rb (µmol/kg)	Cs (nmol/kg)	V (nmol/kg)	Mo (nmol/kg)	U (nmol/kg)	Phosphate (µmol/kg)	Ammonium (µmol/kg)
Bottom seawater	0	10.1	1.37	2.2	38.4	100	13.5		
Yinazao (Blue Moon)*	55	0.9	0.29	3.6	16	10	0.08	2	95
Cerulean Springs	60	2.2	0.45	5.6	25.1	20	0.31		
East Quaker	61	3.7			0.8	198			
Fantangisña (Celestial)*	62	<6	<1	~7.7	~15	~4	0.1	<0.5	~3
NE Quaker	63	<7.64			40.7	50			
Pacman	70	10.1	>1.4	>9.1			<0.28		
Quaker	76	9.39	1.57	96	80.3	36	0.01		
Baby Blue	72	10.5	>1.69	>10.3	5.4	198	<0.54		
Asùt Tesoro (Big Blue)*	72	13	6.6	160	100	104	0.3	3	180
South Chamorro	78	19	10	53.5	16.3	24	<0.1		
Conical	86	15	7.8	>61.6	113	42	0		

depths greater than 8 meters below seafloor (mbsf) in Hole U1492C, with the exception of Section 366-U1492C-16F-1 (Table **T2**). The trace element concentration-depth profiles were significantly influenced by diagenetic reactions near the seafloor; thus, the deep-sourced fluid composition was calculated based on the average concentration of samples deeper than 17 mbsf (V, Rb, and Cs), 31 mbsf (Cs), and 77 mbsf (Mo, Ba, and alkalinity).

The composition of the deep-sourced fluid that upwells near the summit of Fantangisña Seamount was estimated from pore water samples collected from Holes U1497A and U1497B (Table **T2**). Unfortunately, there was no clearly defined asymptotic composition with depth, which is an indication that seepage is slower here than at the other summit sites, allowing diagenetic reactions to dominate trace element depth profiles. Thus, concentrations of dissolved ions in the deep-sourced fluid are generally reported as minimum or maximum values for Fantangisña Seamount.

Concentration-depth profiles reach an asymptote in samples from Holes U1496A and U1496B (Asùt Tesoro Seamount). Data from Hole U1496C were not used in this analysis because these samples were collected using RCB drilling, which resulted in less than ideal cores from which pore waters were extracted. Deep-sourced fluids were calculated from averages of samples that were deeper than 5 mbsf (Hole U1496A) and 3 mbsf (Hole U1496B), with the exception of Sections 366-U1496A-8F-3, 366-U1496A-9F-1, and 366-U1496B-7F-1; each of these three samples was contaminated with drilling fluid (seawater). Similarly, the WSTP sample from Hole U1496C was contaminated with seawater. Because Mo

data from Hole U1496B do not show an asymptote with depth, only data from Hole U1496B were used to estimate the deep-sourced fluid concentration for this element.

Results
Concentration-depth profiles

Concentration-depth profiles for Li, Rb, and Cs and for V, Mo, U, and Ba are presented in Figures **F2** and **F3**, respectively. These profiles highlight differences in composition among the three serpentinite seamounts. In general, fluids from summit sites show a trend from lower Rb, B, and Cs concentrations in fluids from Yinazao Seamount to Fantangisña Seamount and Asùt Tesoro Seamount (i.e., from the shallowest to the deeper source fluids). Chemical compositions of upwelling fluids from summit sites are generally similar for Li and U. Trends for the more reactive elements V and Mo are less defined but are similar at Yinazao and Fantangisña Seamounts and generally greater at Asùt Tesoro Seamount. Ba trends generally match the inverse in the sulfate data, which show a range in values from a low at Fantangisña Seamount to a high at Asùt Tesoro Seamount (Figure **F4**).

In addition, there are some general differences in concentration-depth profiles between summit and flank sites for a given serpentinite mud volcano. In general, flank sites have higher Li concentrations, consistent with diffusive exchanges of Li in bottom seawater. Likewise, Rb concentrations at flank sites are generally more similar to bottom seawater than concentrations in deep-

Figure F2. Pore water concentration depth profiles for Li, Rb, and Cs from Yinazao, Fantangisña, and Asùt Tesoro Seamounts. Solid symbols = summit data (Holes U1492C, U1497A, and U1496A), open symbols = data from the other summit and flank holes, black solid symbol = bottom seawater.
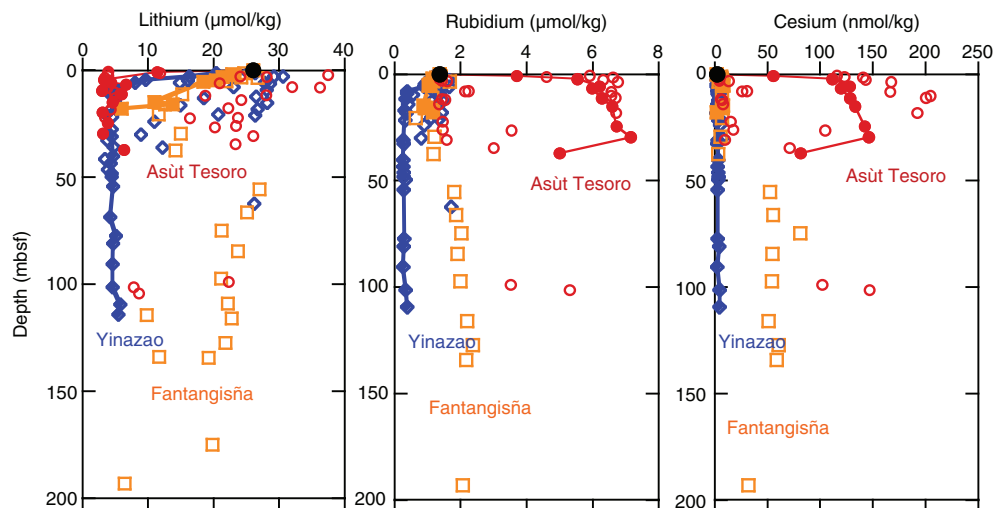

Figure F3. Pore water concentration depth profiles for V, Mo, U, and Ba from Yinazao, Fantangisña, and Asùt Tesoro Seamounts. Solid symbols = summit data (Holes U1492C, U1497A, and U1496A), open symbols = data from the other summit and flank holes, black solid symbol = bottom seawater.
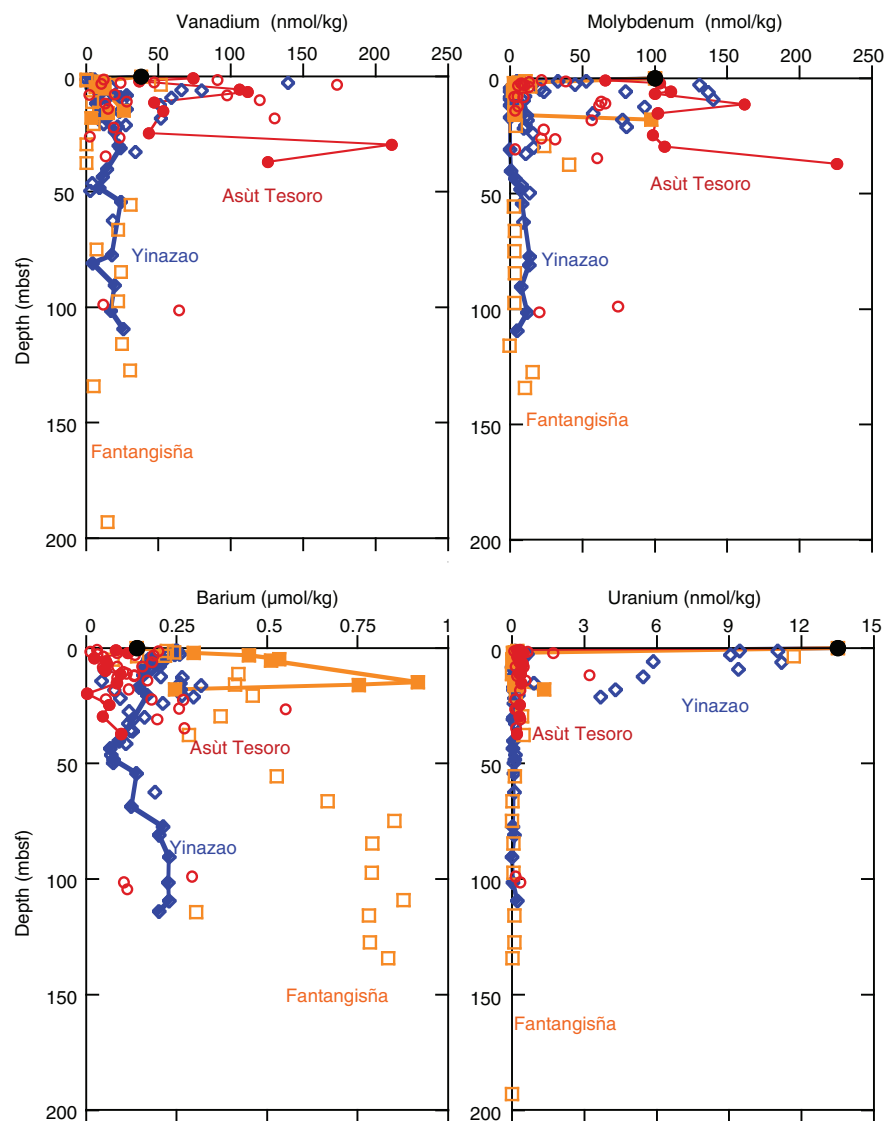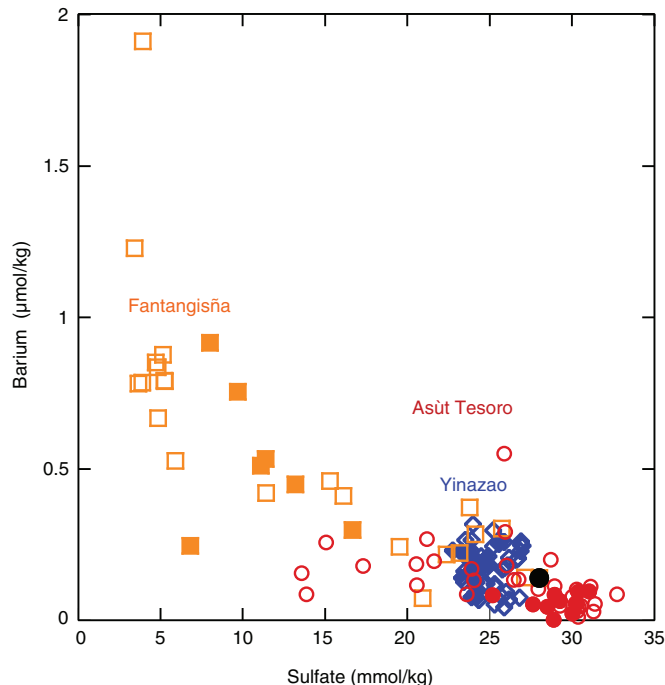
Figure F4. Pore water concentration of sulfate plotted versus Ba from Yinazao, Fantangisña, and Asùt Tesoro Seamounts. Solid symbols = summit data (Holes U1492C, U1497A, and U1496A), open symbols = data from the other summit and flank holes, black solid symbol = bottom seawater.

waters from the flanks of the seamounts have Ba concentrations that mirror the sulfate concentrations but without a clear distinction between flank and summit concentrations. Plots of Mo or V concentrations versus Ba concentrations (not shown) show two distinct groupings, similar to sulfate (Figure F4). One grouping is high in Mo or V and low in Ba, and the other is high in Ba and low in Mo or V, consistent with different modes of production and removal of these elements (e.g., Crusius et al., 1996; Morford et al., 2005; McManus et al., 1998).

Trends in deep-sourced fluids

The distance between the Mariana serpentinite mud volcanoes and the trench is a proxy for the depth to the subduction channel (Mottl et al., 2004; Hulme et al., 2010). In general, the greater this distance, the deeper the source for the upwelling pore fluids and the warmer the temperature in the subduction channel. The range of temperatures below these serpentinite mud volcanoes spans 80°–350°C, affecting the type and rate of reactions that occur at depth (Hulme et al., 2010). Thus, one anticipates changes in the fluid composition as a function of distance from the trench. For example, two noteworthy changes are observed in the Ca and alkalinity data. Close to the trench, Ca concentrations are higher than seawater values and the alkalinity is well below the seawater value (Table T2). In contrast, Ca concentrations farther from the trench are below the seawater value and alkalinity values are high. These values are a result of the temperature dependence of the decarbonization process within the subduction channel (Fryer, Pearce, Stokking, et al., 1999). Likewise, trends are observed in the trace element data.

In general, Rb and Cs concentrations increase in the estimated deep-sourced fluids as a function of distance from the trench, consistent with expectation of seawater-basalt reactions in the subduction channel at increasing temperature (Figure F5A) (You et al., 1996; Sadofsky and Bebout, 2003). In contrast, concentrations of Ba may decrease with distance from the trench, inverse to the sulfate trend (Figure F5B). However, trends of deep-sourced fluid concentrations with distance from the trench were not observed with the other trace element data (Li, V, and Mo), and each of the deep-sourced fluids has U concentrations that approach the limit of detection. Other trends were identified in concentration-concentration plots of various elements (Figure F6). Some of these trends (e.g., K versus Rb) likely reflect changes in the temperature of reaction, whereas others (e.g., Ba versus V) likely reflect redox conditions. Combined, these trends provide a conceptual illustration of subsurface processes and their surface expression (Figure F7).

sourced fluids. Similarly, Cs concentrations at flank sites on Yinazao Seamount are more seawater-like than the sourced fluids; however, flank fluids from Fantangisña Seamount are much higher in Cs than either bottom seawater or the upwelling fluid from the summit. Also, Cs concentrations from the flanks of Yinazao Seamount are nearly identical to their deep-sourced counterparts; both are ~1 nmol/kg different from seawater. Some flank fluids from the upper 20 mbsf have higher U concentrations than the deep-sourced fluid but generally merge with the low concentrations of the deep-sourced fluid, indicative of ongoing removal of seawater U that is diffusively transported into the serpentinite matrix. Concentrations of Mo in the upper 20 mbsf are generally higher than their deep-sourced counterparts, consistent with diagenetic or microbial mediated reactions within this depth zone. Similar diagenetic influences are evident in the V data from Asùt Tesoro Seamount, but a clear delineation is not evident at the other two seamounts. Pore

Figure F5. Concentrations of deep-sourced fluids as a function of distance to the trench. A. Trends in Rb (green circles) and Cs (red squares) are similar, showing increased concentrations with distance and by supposition depth to the subduction channel and temperature within the subduction channel. B. Trends in sulfate (green circles) and Ba (red squares) show an inverse relationship.
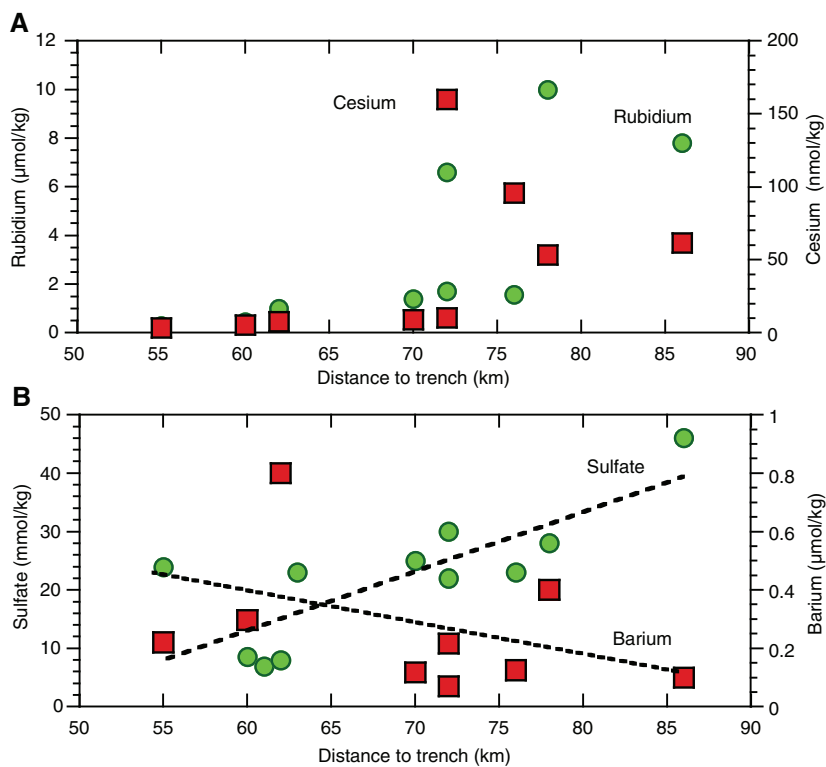

Figure F6. Concentrations of K versus Rb and Ba versus V in deep-sourced fluids. The K-Rb trend is likely due to changes in reactions with increased temperature, and the Ba-V trend is likely redox related.
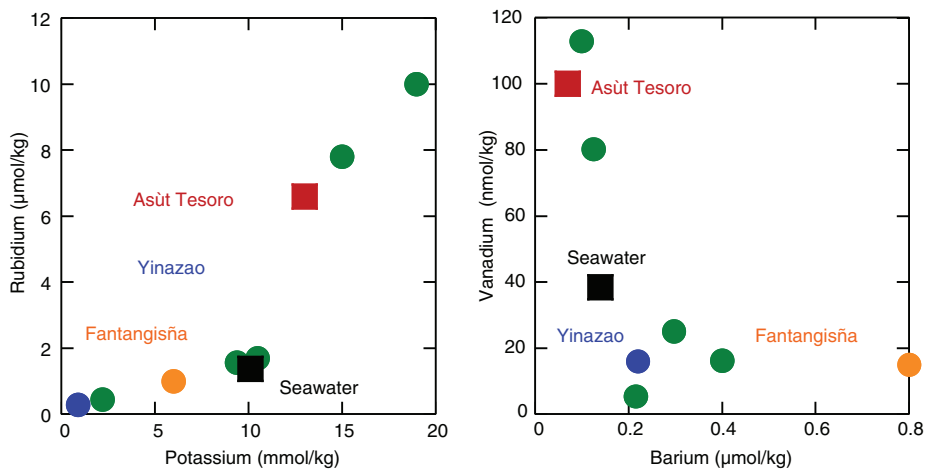
Figure F7. Pore water chemical data derived from the Mariana forearc during Expedition 366, data from this report, and data from two other serpentinite mud volcanoes at a greater distance from the trench (South Chamorro and Conical Seamounts) (Hulme et al., 2010). Bar graphs illustrate relative differences in concentrations among sites to highlight these differences. Depths are conceptual and for illustrative purposes only. (See the Expedition 366 summary chapter [Fryer et al., 2018b].)
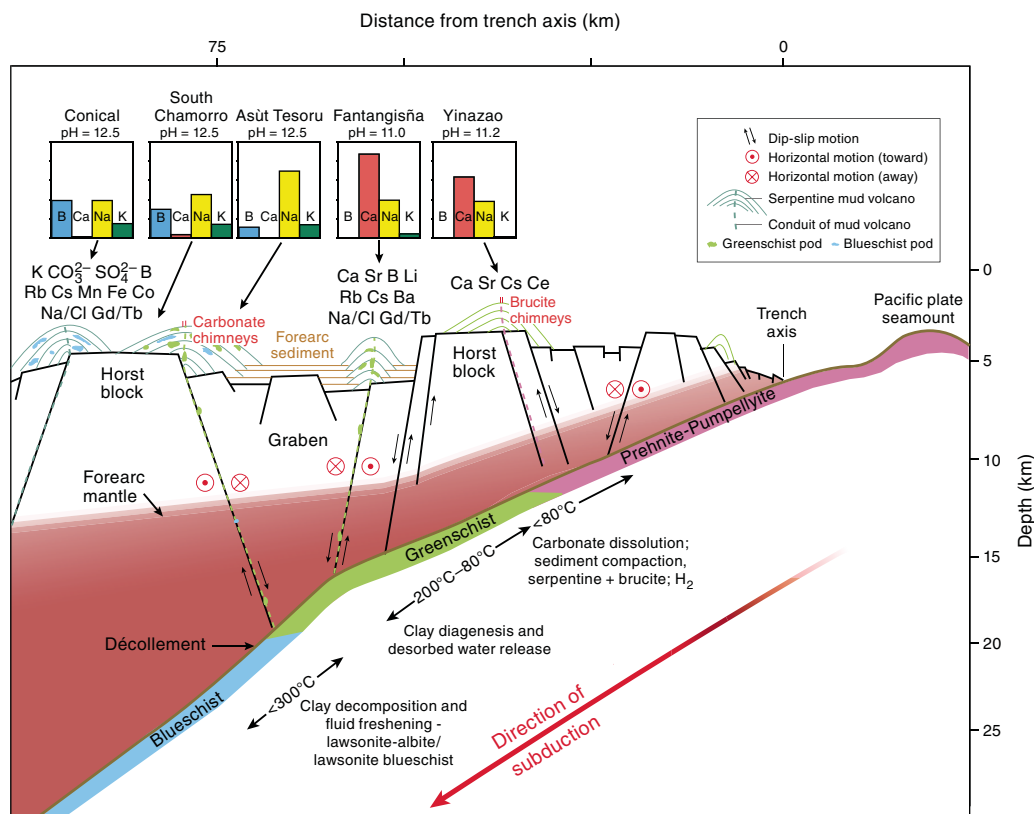
Acknowledgments

References

Crusius, J., Calvert, S., Pedersen, T., and Sage, D., 1996. Rhenium and molybdenum enrichments in sediments as indicators of oxic, suboxic and sulfidic conditions of deposition. *Earth and Planetary Science Letters*, 145(1–4):65–78. https://doi.org/10.1016/S0012-821X(96)00204-X

Fryer, P., Pearce, J.A., Stokking, L.B., et al., 1990. *Proceedings of the Ocean Drilling Program, Initial Reports*, 125: College Station, TX (Ocean Drilling Program). https://doi.org/10.2973/odp.proc.ir.125.1990

Fryer, P., Wheat, C.G., and Mottl, M.J., 1999. Mariana blueschist mud volcanism: implications for conditions within the subduction zone. *Geology*, 27(2):103–106. https://doi.org/10.1130/0091-7613(1999)027<0103:MBMVIF>2.3.CO;2

Fryer, P., Wheat, C.G., Williams, T., Albers, E., Bekins, B., Debret, B.P.R., Deng, J., Dong, Y., Eickenbusch, P., Frery, E.A., Ichiyama, Y., Johnson, K., Johnston, R.M., Kevorkian, R.T., Kurz, W., Magalhaes, V., Mantovanelli, S.S., Menapace, W., Menzies, C.D., Michibayashi, K., Moyer, C.L., Mullane, K.K., Park, J.-W., Price, R.E., Ryan, J.G., Shervais, J.W., Sissmann, O.J., Suzuki, S., Takai, K., Walter, B., and Zhang, R., 2018a. Expedition 366

methods. *In* Fryer, P., Wheat, C.G., Williams, T., and the Expedition 366 Scientists, *Mariana Convergent Margin and South Chamorro Seamount*. Proceedings of the International Ocean Discovery Program, 366: College Station, TX (International Ocean Discovery Program). https://doi.org/10.14379/iodp.proc.366.102.2018

Fryer, P., Wheat, C.G., Williams, T., Albers, E., Bekins, B., Debret, B.P.R., Deng, J., Dong, Y., Eickenbusch, P., Frery, E.A., Ichiyama, Y., Johnson, K., Johnston, R.M., Kevorkian, R.T., Kurz, W., Magalhaes, V., Mantovanelli, S.S., Menapace, W., Menzies, C.D., Michibayashi, K., Moyer, C.L., Mullane, K.K., Park, J.-W., Price, R.E., Ryan, J.G., Shervais, J.W., Sissmann, O.J., Suzuki, S., Takai, K., Walter, B., and Zhang, R., 2018b. Expedition 366 summary. *In* Fryer, P., Wheat, C.G., Williams, T., and the Expedition 366 Scientists, *Mariana Convergent Margin and South Chamorro Seamount*. Proceedings of the International Ocean Discovery Program, 366: College Station, TX (International Ocean Discovery Program). https://doi.org/10.14379/iodp.proc.366.101.2018

Hulme, S.M., Wheat, C.G., Fryer, P., and Mottl, M.J., 2010. Pore water chemistry of the Mariana serpentinite mud volcanoes: a window to the seismogenic zone. *Geochemistry, Geophysics, Geosystems*, 11(1):Q01X09. https://doi.org/10.1029/2009GC002674

McManus, J., Berelson, W.M., Klinkhammer, G.P., Johnson, K.S., Coale, K.H., Anderson, R.F., Kumar, N., Burdige, D.J., Hammond, D.E., Brumsack, H.J., McCorkle, D.C., and Rushdi, A., 1998. Geochemistry of barium in marine sediments: implications for its use as a paleoproxy. *Geochimica et Cosmochimica Acta*, 62(21–22):3453–3473. https://doi.org/10.1016/S0016-7037(98)00248-8

Morford, J.L., Emerson, S.R., Breckel, E.J., and Kim, S.H., 2005. Diagenesis of oxyanions (V, U, Re, and Mo) in pore waters and sediments from a continental margin. *Geochimica et Cosmochimica Acta*, 69(21):5021–5032. https://doi.org/10.1016/j.gca.2005.05.015

Mottl, M.J., Komor, S.C., Fryer, P., and Moyer, C.L., 2003. Deep-slab fluids fuel extremophilic Archaea on a Mariana forearc serpentinite mud volcano: Ocean Drilling Program Leg 195. *Geochemistry, Geophysics, Geosystems,* 4:9009. **https://doi.org/10.1029/2003GC000588**

Mottl, M.J., Wheat, C.G., Fryer, P., Gharib, J., and Martin, J.B., 2004. Chemistry of springs across the Mariana forearc shows progressive devolatilization of the subducting plate. *Geochimica et Cosmochimica Acta,* 68(23):4915–4933. **https://doi.org/10.1016/j.gca.2004.05.037**

Sadofsky, S.J., and Bebout, G.E., 2003. Record of forearc devolatilization in low-T, high-P/T metasedimentary suites: significance for models of convergent margin chemical cycling. *Geochemistry, Geophysics, Geosystems,* 4(4):9003–9031. **https://doi.org/10.1029/2002GC000412**

Salisbury, M.H., Shinohara, M., Richter, C., et al., 2002. *Proceedings of the Ocean Drilling Program, Initial Reports,* 195: College Station, TX (Ocean Drilling Program). **https://doi.org/10.2973/odp.proc.ir.195.2002**

Wheat, C.G., Fryer, P., Fisher, A.T., Hulme, S., Jannasch, H., Mottl, M.J., and Becker, K., 2008. Borehole observations of fluid flow from South Chamorro Seamount, an active serpentinite mud volcano in the Mariana forearc. *Earth and Planetary Science Letters,* 267(3–4):401–409. **https://doi.org/10.1016/j.epsl.2007.11.057**

Wheat, C.G., Jannasch, H.W., Fisher, A.T., Becker, K., Sharkey, J., and Hulme, S., 2010. Subseafloor seawater-basalt-microbe reactions: continuous sampling of borehole fluids in a ridge flank environment. *Geochemistry, Geophysics, Geosystems,* 11(7):Q07011. **https://doi.org/10.1029/2010GC003057**

You, C.-F., Castillo, P.R., Gieskes, J.M., Chan, L.H., and Spivack, A.J., 1996. Trace element behavior in hydrothermal experiments: implications for fluid processes at shallow depth in subduction zones. *Earth and Planetary Science Letters,* 140(1–4):41–52. **https://doi.org/10.1016/0012-821X(96)00049-0**